Electronic Reconstruction in $(LaVO_3)_m/SrVO_3$ (m = 5, 6) Superlattices

*Qingqing Dai, Ulrike Lüders, Raymond Frésard, Ulrich Eckern, and Udo Schwingenschlögl**

The $(LaV^{3+}O_3)_m/SrV^{4+}O_3$ (m = 5, 6) superlattices are investigated by first principles calculations. While bulk $LaVO_3$ is a C-type antiferromagnetic semiconductor and bulk $SrVO_3$ is a paramagnetic metal, semiconducting A-type antiferromagnetic states for both superlattices are found due to epitaxial strain. At the interfaces, however, the V spins couple antiferromagnetically for m = 5 and ferromagnetically for m = 6 (m-dependence of the magnetization). Electronic reconstruction in form of charge ordering is predicted to occur with V^{3+} and V^{4+} states arranged in a checkerboard pattern on both sides of the SrO layer. As compared to bulk $LaVO_3$, the presence of V^{4+} ions introduces in-gap states that strongly reduce the bandgap and influence the orbital occupation and ordering.

1. Introduction

Superlattices of transition metal oxides have been widely investigated in recent years, as they host a number of physical phenomena and functionalities that are not found in the bulk oxides, which is attributed to charge, spin, and orbital reconstructions.[1–4] The crystal structure, electronic properties, magnetism, and transport behavior of $LaVO_3/SrVO_3$ superlattices with varying periodicities have been described in refs.[5–10] In particular, ferromagnetism with Curie temperature far above room temperature has been evidenced, which is striking, because doping of bulk $LaVO_3$ never results in a ferromagnetic phase. Indeed, bulk $LaVO_3$ is a Mott-Hubbard insulator[11,12] with a phase transition at ≈140 K that leads from monoclinic to orthorhombic symmetry and from a C-type antiferromagnetic (AFM) to a paramagnetic state.[13] In contrast, bulk $SrVO_3$ is a paramagnetic metal with cubic symmetry.[14] The electronic configurations of the V ions in $LaVO_3$ and $SrVO_3$, respectively, are $3d^2$ (V^{3+}) and $3d^1$ (V^{4+}). It has been found that the solid solution $La_{1-x}Sr_xVO_3$, containing mixed V^{3+} and V^{4+} states, shows a non-Fermi liquid behavior up to very high temperatures and is subject to an insulator-to-metal transition under hole doping.[15,16]

Appearance of both V^{3+} and V^{4+} states at the interfaces of $(LaVO_3)_6/(SrVO_3)_3$ superlattices has been reported in ref. [10] without identifying a specific spatial pattern. In addition, it is known that the magnetization in $(LaVO_3)_m/SrVO_3$ superlattices depends on the thickness of the $LaVO_3$ layer, with m = 4, 6 yielding larger saturation magnetization than m = 3, 5.[6] The fact that in the latter case the saturation magnetization does not exceed the threshold of the substrate impurities indicates that there is no macroscopic magnetization. The mechanism responsible for the deviating behaviors of superlattices with odd and even thicknesses is not fully understood so far. While it could be a pure strong correlation effect,[17] results on the bulk compounds indicate that strain introduced into the superlattices by the substrate may also influence the magnetic behavior (as well as other physical properties).[18] Distortions in vanadate superlattices generated by charge disproportionation into V^{3+} and V^{4+} ions have the potential to result in ferroelectricity[19] and distortions of the VO_6 octahedra can have complex effects on the orbital occupations.[20]

Based on these considerations, we will study in the present work $(LaVO_3)_m/SrVO_3$ superlattices by numerical calculations within density functional theory, using experimental lattice parameters. Our considerations will focus on the cases m = 5 and 6, as examples for superlattices with odd and even thicknesses. We will establish the magnetic ground state, provide detailed insight into the electronic reconstruction (in particular with respect to the V ions at the interfaces of the superlattices), and explain the observed m-dependence of the electronic and magnetic properties.

2. Methodology

Spin-polarized first-principles calculations are performed employing the projector augmented wave method of the Vienna

Dr. Q. Dai, Prof. U. Schwingenschlögl
Physical Science and Engineering Division (PSE)
King Abdullah University of Science and Technology (KAUST)
Thuwal 23955-6900, Saudi Arabia
E-mail: udo.schwingenschlogl@kaust.edu.sa
Dr. U. Lüders, Prof. R. Frésard
Normandie Université
ENSICAEN, UNICAEN, CNRS, CRISMAT
14000 Caen, France
Prof. U. Eckern
Institut für Physik
Universität Augsburg
86135 Augsburg, Germany
The ORCID identification number(s) for the author(s) of this article can be found under https://doi.org/10.1002/admi.201701169.

DOI: 10.1002/admi.201701169

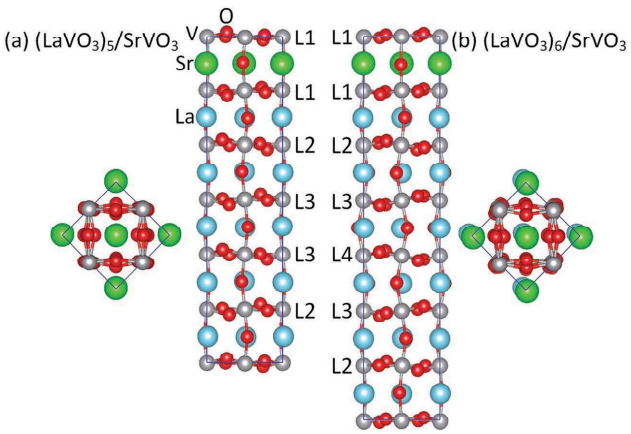

Figure 1. Relaxed structures of the $m = 5$ and $m = 6$ superlattices.

Ab initio Simulation Package.[21] The generalized gradient approximation (GGA) in the Perdew–Burke–Ernzerhof flavor is used for the exchange-correlation functional. To describe the onsite electronic correlations of the V 3*d* orbitals the GGA+*U* approach[22] is adopted with an effective interaction parameter of 3 eV (to reproduce the experimental bandgap of bulk $LaVO_3$[18,23]). The cut-off energy of the plane-wave basis is set to 500 eV and the Brillouin zone is sampled on $9 \times 9 \times 1$ and $12 \times 12 \times 2$ k-meshes in the structure optimizations and electronic structure calculations, respectively. Electronic self-consistency of 10^{-5} eV is achieved and the atomic positions are relaxed until no atom experiences a residual force above 0.02 eV $Å^{-1}$.

According to experiments, the pseudocubic lattice parameter of $LaVO_3$ is 3.92 Å and the cubic lattice parameter of $SrVO_3$ is 3.84 Å.[5] It has been reported that $(LaVO_3)_m/SrVO_3$ superlattices grown on $SrTiO_3$ substrate develop a small tetragonal distortion of the perovskite structure with an in-plane lattice parameter of $a = 3.88$ Å and an out-of-plane lattice parameter $c = 3.95$ Å.[6] Recent theoretical studies on $LaVO_3/SrVO_3$ superlattices have assumed a different tetragonal distortion ($c/a < 1$)[19] or have employed bulk symmetry.[20] Using the experimental lattice parameters will allow us to be more realistic, which is particularly important for $LaVO_3$, since the c/a ratio in this compound has strong effects on the electronic properties.[18] In unstrained bulk $LaVO_3$ the magnetic ground state is given by C-type AFM ordering,[12] while strain can induce G and A-type AFM ordering.[18] In order to identify the magnetic ground state for the $(LaVO_3)_m/SrVO_3$ superlattices, we therefore study A, C, and G-type AFM ordering as well as ferromagnetic (FM) ordering. To this aim, we built $\sqrt{2} \times \sqrt{2} \times 6$ ($m = 5$) and $\sqrt{2} \times \sqrt{2} \times 7$ ($m = 6$) supercells of the perovskite unit cell, see **Figure 1**, based on the experimental lattice parameters mentioned above.

3. Results and Discussion

We obtain in both superlattices for A-type AFM ordering the lowest total energy, 142 meV ($m = 5$) and 126 meV ($m = 6$) lower than for C-type AFM ordering, 294 meV ($m = 5$) and 132 meV ($m = 6$) lower than for G-type AFM, and 173 meV ($m = 5$) and 221 meV ($m = 6$) lower than for FM ordering. This fact indicates that the epitaxial strain present in the superlattices due to the substrate yields a magnetic phase transition away from the C-type AFM ordering of bulk $LaVO_3$. A-type AFM ordering also appears in bulk $LaVO_3$ for a corresponding c/a ratio and results in partial occupation of the d_{xy} orbitals.[18] This implies that the superlattices under study might also deviate from the bulk orbital ordering (d_{xy} occupied, $d_{xz/yz}$ G-type ordered[24]).

The optimized structures obtained for the $m = 5$ and $m = 6$ superlattices in the case of A-type AFM ordering (ground state) are shown in Figure 1a,b, respectively. For convenience, the VO_2 layers are counted starting from the SrO layer. Both superlattices show substantial distortions of the VO_6 octahedra, see **Table 1**, which lists the out-of-plane V—O bond lengths between adjacent atomic layers and the corresponding V—O—V bond angles (averaged over all bonds or bond angles between these layers). Both short (1.84 Å, 1.83 Å) and long (2.04 Å, 2.03 Å) V—O bonds appear between the L1 and SrO layers for both superlattices. These bond lengths correspond to V^{3+} (long) and V^{4+} (short) ions, as we will discuss later. Further away from the SrO layer all V—O bond lengths are very similar, see Table 1, while the V—O—V bond angles decrease and approach the bulk value of 157°.[25] We note that the pinching effect (shortening of the V—O bonds next to the SrO layer) discovered in ref. [26] by simulations for $1 \times 1 \times 6$ and $1 \times 1 \times 7$ supercells is qualitatively reproduced by our $\sqrt{2} \times \sqrt{2} \times 6$ and $\sqrt{2} \times \sqrt{2} \times 7$ supercells, however, with significant changes in magnitude and with a strongly modified pattern of bond lengths across the supercells. In addition, the realization of both short and long V—O bonds between the L1 and SrO layers is simply not possible in the smaller supercells of ref. [26]. This shows that the computationally expensive approach of the present study is essential for describing key structural features, besides opening the possibility to consider in-plane magnetic ordering.

We find for the VO_6 octahedra rotations of about 10° around the *c*-axis, while those around the *a*- and *b*-axes are not significant. This resembles observations for $LaVO_3$ thin films on $SrTO_3$[27], again in response to the presence of compressive strain. Concerning the L1 layers next to the SrO layer, the $m = 5$ superlattice shows a reduction of the rotation angles, while the $m = 6$ superlattice does not. However, the octahedral distortions

Table 1. Out-of-plane V—O bond lengths and V—O—V bond angles between the atomic layers of the superlattices.

	$m = 5$		$m = 6$	
SrO–L1	1.84 Å	2.04 Å	1.83 Å	2.03 Å
L1–LaO	2.00 Å		1.99 Å	
LaO–L2	2.02 Å		2.01 Å	
L2–LaO	2.02 Å		2.02 Å	
LaO–L3	2.03 Å		2.02 Å	
L3–LaO	2.03 Å		2.03 Å	
LaO–L4			2.03 Å	
L1-SrO-L1	163°		172°	
L1-LaO-L2	160°		164°	
L2-LaO-L3	159°		159°	
L3-LaO-L4			157°	

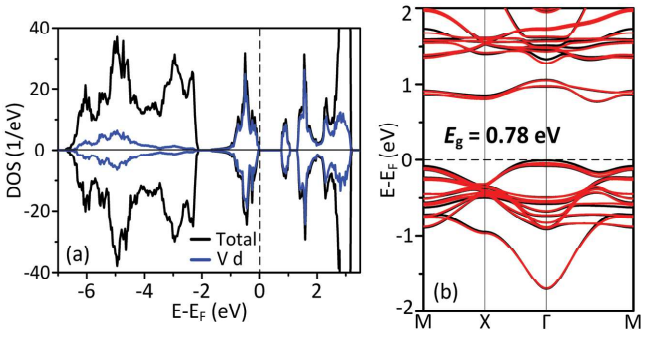

Figure 2. DOS and band structure of the $m = 5$ superlattice. The black and red lines on the right hand side denote the spin majority and minority bands, respectively.

in the L1 layers (see above) jeopardize an analysis in terms of rotations (collective displacements of O atoms). Therefore, it seems that the strong distortions of half of the VO_6 octahedra in the L1 layers are the principal contributors to the structure stabilization around the Sr ions, allowing for a nearly bulk-like structure in the other VO_2 layers.

The density of states (DOS) and band structure obtained for the $m = 5$ superlattice are shown in **Figures 2**a,b, respectively. According to the DOS, the V 3*d* states dominate at the valence band edge and therefore play a decisive role for the electronic properties. The bandgap turns out to be 0.78 eV, i.e., much smaller than the bulk value of 1.39 eV calculated by the same method. The reason is that two in-gap hole bands, see Figure 2b, are introduced in the bandgap of bulk $LaVO_3$ due to partial replacement of La^{3+} by Sr^{2+} in the superlattice.

Figure 3a–e gives the orbital-projected V 3*d* DOS for layers L1, L2, and L3. We sum here the V 3*d* DOS for the two L1 layers, two L2 layers, and two L3 layers, see Figure 1, because the differences encountered for the two sides of the SrO layer are small. We find that the occupied states always are dominated by the t_{2g} orbitals (d_{xy}, d_{yz}, and d_{xz}), whereas the e_g orbitals (d_{3z2-r2} and d_{x2-y2}) appear at higher energy and thus play no role for the following discussion. The L1 layer (directly in contact with the SrO layer) shows distinct differences in the orbital occupations with respect to the L2 and L3 layers, see particularly Figure 3b,c, because the in-gap hole bands turn out to belong to the d_{yz} and d_{xz} orbitals of the L1 layer.

To further explore the origin of the hole states, the DOS is projected on the individual V atoms in the two L1 layers in **Figure 4**a–d. AFM ordering between the L1 layers is evident. For atom V1a (V1*d*) only the d_{xy} orbital is occupied by one spin-up (spin-down) electron, resulting in a magnetic moment of 1.0 μ_B. This $3d^1$ electronic configuration corresponds to the V^{4+} state of bulk $SrVO_3$. For atom V1b (V1c) both the d_{xz} and d_{yz} orbitals are occupied by one spin-up (spin-down) electron, whereas the d_{xy} orbital remains empty. This inversion of the orbital occupation between the V^{3+} and V^{4+} ions can be understood in terms of the observed octahedral distortions, see above, because the short V—O bonds favor the in-plane orbital (V^{4+}) and the long V—O bonds the out-of-plane orbitals (V^{3+}). The magnetic moment of 1.8 μ_B obtained for atoms V1b and V1c is very close to that of the V^{3+} state of bulk $LaVO_3$ (1.8–2.0 μ_B),[28] confirming a $3d^2$ electronic configuration. We note that the

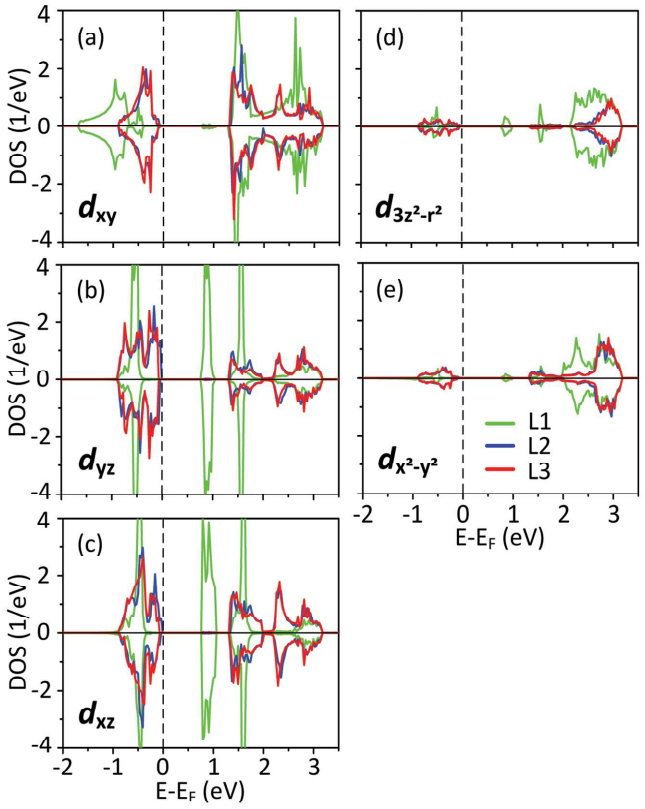

Figure 3. V 3*d* DOS projected on VO_2 layers L1, L2, and L3 of the $m = 5$ superlattice.

main features of the V 3*d* t_{2g} DOS in the V^{3+} and V^{4+} states and the respective magnetic moments are consistent with previous results on the $m = 1$ superlattice.[19]

Figure 4e–h shows the DOS projected on the V atoms in the L2 and L3 layers following the layer with atoms V1c and V1d. Corresponding results for the L2 and L3 layers on the other side of the SrO layer are very similar and therefore omitted here. We observe AFM ordering between the L1 and L2 layers as well as between the L2 and L3 layers. Combined with the in-plane FM ordering evident in Figure 4, this gives rise to an overall A-type AFM state. The fact that we have in the valence band contributions of all three t_{2g} orbitals agrees with the prediction of ref. [17] for bulk $LaVO_3$ in the presence of a tetragonal distortion with c/a > 1. Indeed, we find in the L2 and L3 layers magnetic moments of 1.8 μ_B and, therefore, $3d^2$ electronic configurations. It is important to realize that we have in the $m = 5$ superlattice an even number of VO_2 layers, compare Figure 1, so that the A-type AFM ordering results in zero macroscopic magnetization. While in the L1 layers V^{3+} and V^{4+} states are arranged in a checkerboard pattern, elsewhere the V^{3+} state of bulk $LaVO_3$ is maintained.

We will show below that A-type AFM ordering is also realized in the $m = 6$ superlattice. However, due to the odd number of VO_2 layers in this superlattice at least two layers must be subject to FM ordering, which is confirmed by the experimental observation of finite macroscopic magnetization.[6] FM alignment of the two L1 layers turns out to be energetically favorable over FM alignment of the L1 and L2 layers by 30 meV and over

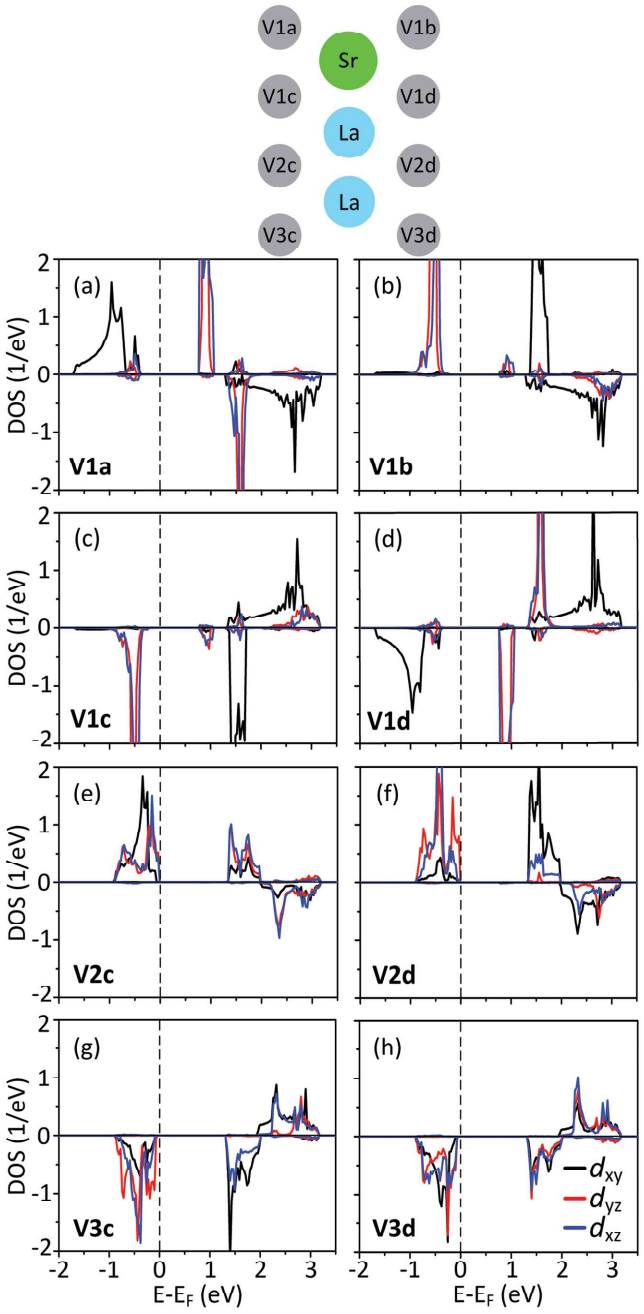

Figure 4. V 3*d* t_{2g} DOS of individual V atoms in the $m = 5$ superlattice.

FM alignment of the L2 and L3 layers by 60 meV (and therefore is studied in the following). The DOS and band structure obtained for the $m = 6$ superlattice are shown in **Figure 5**a,b, respectively. Similar to the $m = 5$ superlattice, the V 3*d* states turn out to dominate at the valence band edge. However, all in-gap states now belong to the same spin channel and a net magnetic moment of 2 μ_B is obtained for the supercell. As this value agrees with the experimental situation,[6] we conclude that the appearance of macroscopic magnetization is a direct consequence of the epitaxial strain that leads to A-type AFM ordering. FM ordering of the L1 layers in the $m = 6$ superlattice

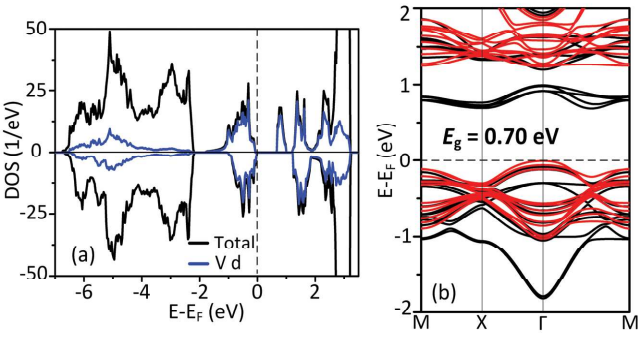

Figure 5. DOS and band structure of the $m = 6$ superlattice. The black and red lines on the right hand side denote the spin majority and minority bands, respectively.

is also in line with the fact that the V—O—V bond angles in Table 1 reflect different rotation patterns of the VO_6 octahedra in the two superlattice, which are linked to the magnetic exchange coupling.[29]

Except for minor differences in the magnetic moments, the electronic reconstruction otherwise is very similar in the $m = 5$ and $m = 6$ superlattices. In particular, this is seen in the orbital-projected V 3*d* DOS given in **Figure 6**a–e for the different VO_2 layers (again summed for layers with the same distance to the SrO layer, see Figure 1, due to close similarity): The occupied states mainly trace back to the t_{2g} orbitals, the d_{xy} states in the L1 layer (next to the SrO layer) appear at lower energy than in

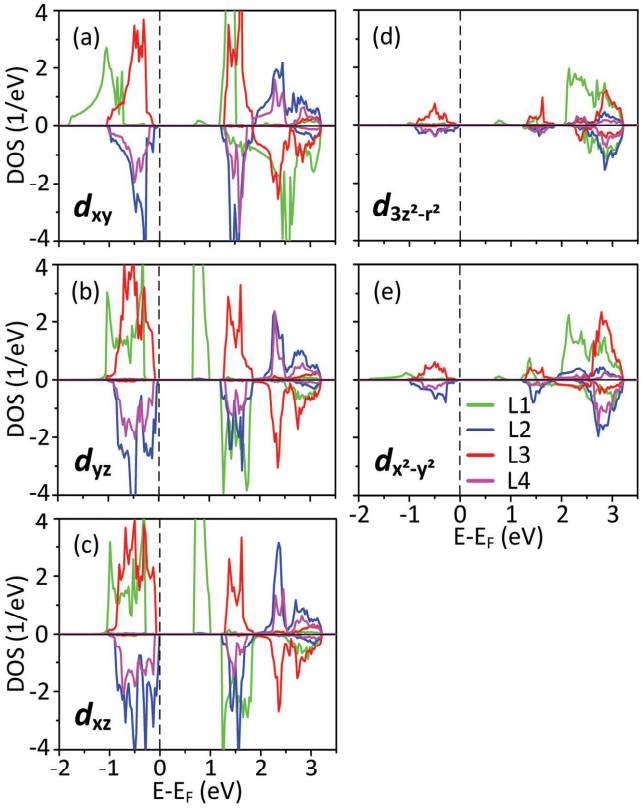

Figure 6. V 3*d* DOS projected on VO_2 layers L1, L2, L3, and L4 of the $m = 6$ superlattice.

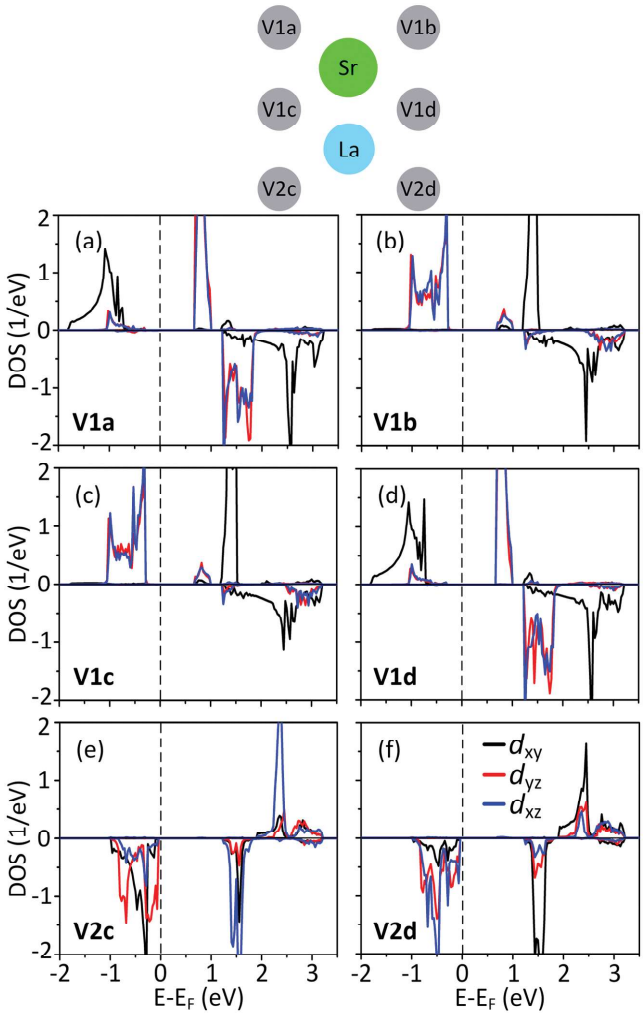

Figure 7. V 3*d* t_{2g} DOS of individual V atoms in the $m = 6$ superlattice.

the other layers, and the in-gap hole bands belong to the d_{xz} and d_{yz} orbitals of the L1 layer.

Figure 7a–d shows the DOS projected on individual V atoms, reflecting FM ordering of the two L1 layers. The valence states of atoms V1a and V1d are due to the d_{xy} orbital and both short V—O bonds and magnetic moments of 1.0 μ_B are in line with $3d^1$ electronic configurations. On the other hand, the valence states of atoms V1b and V1c trace back to the d_{xz} and d_{yz} orbitals with long V—O bonds and magnetic moments of 1.8 μ_B, resembling the V^{3+} state of bulk $LaVO_3$. We thus obtain also for the $m = 6$ superlattice in the L1 layer a checkerboard pattern of V^{3+} and V^{4+} states. For the V atoms in layers L2, L3, and L4, finally, all three t_{2g} orbitals contribute to the valence band, see Figure 7e,f for an example, and we have long V—O bonds and magnetic moments of 1.8 μ_B as in bulk $LaVO_3$.

We notice that our calculations result in semiconducting characters for both the $m = 5$ and $m = 6$ superlattices. For the $m = 6$ superlattice this fact is supported by AC measurements,[7] whereas in DC measurements[6] a metallic low temperature behavior is found. This difference between experiment and calculations can be explained by the likely presence of O defects in the investigated samples. A recent study of the band structure of O deficient $SrVO_3$ thin films points to complex band shifts due to local modifications of the crystalline structure around O vacancies.[30] In superlattices this excess charge will most probably occupy interface states with high effective mass, explaining the observed discrepancy between experiment and calculations. Moreover, our results for the $m = 5$ and $m = 6$ superlattices clearly point at a checkboard pattern of V^{3+} and V^{4+} states, which is one of the patterns proposed in ref. [19] besides other patterns such as stripe order. At least for the lattice parameters observed experimentally in the case that a single $SrVO_3$ layer is surrounded by thick $LaVO_3$ layers, the checkerboard pattern turns out to be energetically favorable over all other patterns compatible with our choice of supercells.

4. Conclusions

We have studied the electronic reconstruction and magnetic ordering in the $(LaVO_3)_m/SrVO_3$ ($m = 5, 6$) superlattices with odd and even thicknesses of the $LaVO_3$ region. We find in both cases A-type AFM ordering of the V spins, except for FM alignment in the two interfacial VO_2 layers of the $m = 6$ superlattice. A-type AFM ordering of $LaVO_3$, which realizes C-type AFM ordering as bulk compound, is demonstrated to be a consequence of epitaxial strain induced by the substrate. Differences in the magnetism of the $m = 5$ and $m = 6$ superlattices can be attributed to the fact that only in the case of odd m an even number of VO_2 layers is available to fully realize A-type AFM ordering, which explains the odd-even behavior observed in experiments. For the first time we have identified an electronic reconstruction in the interfacial VO_2 layers with an equal number of V^{3+} and V^{4+} states arranged in a checkerboard pattern, whereas elsewhere the V^{3+} state of bulk $LaVO_3$ is maintained. The V^{4+} ions are responsible for the creation of in-gap hole bands, which will be occupied in O deficient samples.

Acknowledgements

The research reported in this publication was supported by funding from King Abdullah University of Science and Technology (KAUST). It was also supported by the German Science Foundation (DFG) through TRR 80.

Conflict of Interest

The authors declare no conflict of interest.

Keywords

$LaVO_3$, $SrVO_3$, superlattice, transition metal oxide

[1] H. Y. Hwang, Y. Iwasa, M. Kawasaki, B. Keimer, N. Nagaosa, Y. Tokura, *Nat. Mater.* **2012**, *11*, 103.
[2] N. Reyren, S. Thiel, A. D. Caviglia, L. Fitting-Kourkoutis, G. Hammerl, C. Richter, C. W. Schneider, T. Kopp, A.-S. Rüetschi, D. Jaccard, M. Gabay, D. A. Muller, J.-M. Triscone, J. Mannhart, *Science* **2007**, *317*, 1196.
[3] A. Ohtomo, H. Y. Hwang, *Nature* **2004**, *427*, 423.
[4] A. Ohtomo, D. A. Muller, J. L. Grazul, H. Y. Hwang, *Nature* **2002**, *419*, 378.
[5] W. C. Sheets, B. Mercey, W. Prellier, *Appl. Phys. Lett.* **2007**, *91*, 192102.
[6] U. Lüders, W. C. Sheets, A. David, W. Prellier, R. Frésard, *Phys. Rev. B* **2009**, *80*, 241102(R).
[7] D. W. Jeong, W. S. Choi, T. D. Kang, C. H. Sohn, A. David, H. Rotella, A. A. Sirenko, C. H. Lee, J. H. Kim, U. Lüders, W. Prellier, Y.-J. Kim, Y. S. Lee, T. W. Noh, *Phys. Rev. B* **2011**, *84*, 115132.
[8] P. Boullay, A. David, W. C. Sheets, U. Lüders, W. Prellier, H. Tan, J. Verbeeck, G. Van Tendeloo, C. Gatel, G. Vincze, Z. Radi, *Phys. Rev. B* **2011**, *83*, 125403.
[9] A. David, R. Frésard, Ph. Boullay, W. Prellier, U. Lüders, P.-E. Janolin, *Appl. Phys. Lett.* **2011**, *98*, 212106.
[10] H. Y. Tan, R. Egoavil, A. Béché, G. T. Martinez, S. Van Aert, J. Verbeeck, G. Van Tendeloo, H. Rotella, P. Boullay, A. Pautrat, W. Prellier, *Phys. Rev. B* **2013**, *88*, 155123.
[11] T. Arima, Y. Tokura, J. B. Torrance, *Phys. Rev. B* **1993**, *48*, 17006.
[12] T. Mizokawa, A. Fujimori, *Phys. Rev. B* **1996**, *54*, 5368.
[13] P. Bordet, C. Chaillout, M. Marezio, Q. Huang, A. Santoro, S.-W. Cheong, H. Takagi, C. S. Oglesby, B. Batlogg, *J. Solid State Chem.* **1993**, *106*, 253.
[14] V. Giannakopoulou, P. Odier, J. M. Bassat, J. P. Loup, *Solid State Commun.* **1995**, *93*, 579.
[15] S. Miyasaka, T. Okuda, Y. Tokura, *Phys. Rev. Lett.* **2000**, *85*, 5388.
[16] I. C. Lekshmi, A. Gayen, M. S. Hegde, *J. Phys. Chem. Solids* **2005**, *66*, 1647.
[17] R. Frésard, M. Lamboley, *J. Low Temp. Phys.* **2002**, *126*, 1091.
[18] H. M. Weng, K. Terakura, *Phys. Rev. B* **2010**, *82*, 115105.
[19] S. Y. Park, A. Kumar, K. M. Rabe, *Phys. Rev. Lett.* **2017**, *118*, 087602.
[20] J. Varignon, N. C. Bristowe, E. Bousquet, P. Ghosez, *Sci. Rep.* **2015**, *5*, 15364.
[21] G. Kresse, D. Joubert, *Phys. Rev. B* **1999**, *59*, 1758.
[22] S. L. Dudarev, G. A. Botton, S. Y. Savrasov, C. J. Humphreys, A. P. Sutton, *Phys. Rev. B* **1998**, *57*, 1505.
[23] Z. Fang, N. Nagaosa, *Phys. Rev. Lett.* **2004**, *93*, 176404.
[24] S. Miyasaka, Y. Okimoto, Y. Tokura, *J. Phys. Soc. Jpn.* **2002**, *71*, 2086.
[25] H. Sawada, N. Hamada, K. Terakura, T. Asada, *Phys. Rev. B* **1996**, *53*, 12742.
[26] C. Schuster, U. Lüders, R. Frésard, U. Schwingenschlögl, *EPL* **2013**, *103*, 37003.
[27] H. Rotella, U. Lüders, P.-E. Janolin, V. H. Dao, D. Chateigner, R. Feyerherm, E. Dudzik, W. Prellier, *Phys. Rev. B* **2012**, *85*, 184101.
[28] I. Solovyev, N. Hamada, K. Terakura, *Phys. Rev. B* **1996**, *53*, 7158.
[29] H. T. Dang, A. J. Millis, *Phys. Rev. B* **2013**, *87*, 155127.
[30] S. Backes, T. C. Rödel, F. Fortuna, E. Frantzeskakis, P. Le Fèvre, F. Bertran, M. Kobayashi, R. Yukawa, T. Mitsuhashi, M. Kitamura, K. Horiba, H. Kumigashira, R. Saint-Martin, A. Fouchet, B. Berini, Y. Dumont, A. J. Kim, F. Lechermann, H. O. Jeschke, M. J. Rozenberg, R. Valentí, A. F. Santander-Syro, *Phys. Rev. B* **2016**, *94*, 024110.